Hindawi
Mathematical Problems in Engineering
Volume 2022, Article ID 2058258, 19 pages
https://doi.org/10.1155/2022/2058258

Research Article

Bearing Fault Feature Extraction Method Based on GA-VMD and Center Frequency

Yuxing Li[1,2] **Bingzhao Tang**[1] **Xinru Jiang**[1] **and Yingmin Yi**[1,2]

[1]*School of Automation and Information Engineering, Xi'an University of Technology, Xi'an 710048, China*
[2]*Shaanxi Key Laboratory of Complex System Control and Intelligent Information Processing, Xi'an University of Technology, Xi'an 710048, China*

Correspondence should be addressed to Yingmin Yi; yiym@xaut.edu.cn

Received 14 September 2021; Revised 25 November 2021; Accepted 15 January 2022; Published 30 January 2022

Academic Editor: Jian G. Zhou

To promote the effect of variational mode decomposition (VMD) and further enhance the recognition performances of bearing fault signals, genetic algorithm (GA) is applied to optimize the combination of VMD parameters in this paper, and GA-VMD algorithm is put forward to improve the decomposition accuracy of VMD. In addition, combined with the center frequency, a feature extraction method based on GA-VMD and center frequency is proposed to ameliorate the difficulty of bearing fault feature extraction. Firstly, the bearing signal is decomposed into a series of intrinsic mode components (IMFs) by GA-VMD. Then, the Center Frequency of IMFs is extracted, and the recognition rate is calculated by k-nearest neighbor (KNN) algorithm. Simulation signal experiments state clearly that, compared with manual parameter setting-VMD algorithm and parameter optimization VMD algorithm based on particle swarm optimization (PSO), the decomposition result of GA-VMD has a smaller root mean square error and higher decomposition accuracy, which verifies the effectiveness of GA-VMD. The experimental results demonstrate that, by comparison with the feature extraction method based on envelope entropy, the feature extraction method based on center frequency has better inter class separability and higher mean recognition rate (the highest recognition rate of single feature is 94.5%, and in the case of multiple features, the recognition rate reaches 100% when four features are extracted) and can realize the accurate identification of different bearing fault signals.

1. Introduction

As an essential part of various mechanical equipment, bearings have been widely used in civil, industrial, and military applications [1, 2]. However, due to the arduous working conditions, bearings are extremely susceptible to damage [3], which can cause economic losses and even affect personal safety. Simultaneously, the bearing signal in the fault state will produce some periodic transients, which contains the status information of the bearing during operation [4]. Therefore, fault diagnosis of bearings is of great significance to ensure the safe, stable, and reliable operation of mechanical equipment [5, 6].

In recent years, many scholars have put forward their methods for fault diagnosis [7, 8]. Generally speaking, there are two key steps in bearing signal fault diagnosis; the first step is the extracted features. Recently, there are many methods that can be extracted as features and used for fault detection of various types of signals, such as the Lempel-Ziv complexity (LZC) [9], the correlation dimension [10], the Lyapunov exponent [11], and the entropy-based method [12, 13]. Among which, LZC and the entropy-based method can effectively reflect the complexity of the time series and have better robustness and simplicity compared with other features [14, 15]. However, only relying on the separability of the extracted features will be susceptible to interference from noise signals.

Another critical step of bearing signal fault diagnosis is the signal processing method. In 1998, Huang et al. first proposed empirical mode decomposition (EMD) and used it for adaptive decomposition of target signals [16], which has received extensive attention. In 2009, Wu et al. proposed an

ensemble empirical mode decomposition (EEMD) method on the basis of EMD, which can use the statistical properties of white noise to reduce modal aliasing [17, 18]. However, EEMD still belongs to recursive decomposition and is vulnerable to modal aliasing and endpoint effect, so there will be some decomposition errors [19, 20]. In order to solve these problems, Dragomiretskiy et al. proposed the variational modal decomposition (VMD) method in 2014 [21], which can achieve adaptive decomposition of the target signal by iteratively searching for the optimal solution of the variational model, so as to determine the center frequency and bandwidth of each mode. Compared with EMD and EEMD, VMD also has stronger robustness [22–24].

However, different from EMD and its improved algorithm, VMD is more dependent on the setting of parameters, including the number of decomposition layers and penalty factors. In recent years, many scholars have improved VMD [25–27]. Tang Guiji et al. used particle swarm optimization (PSO) algorithm to optimize combination parameters and established a fitness function based on minimum envelope entropy [28]; Mirjalili et al. proposed the whale optimization algorithm (WOA) algorithm in 2016 and proved that it has Strong local and global search ability [29]. In this paper, genetic algorithm (GA) [30, 31] is used as the optimization method, and envelope entropy is selected as the fitness function, and then combined with VMD for automatic optimization of parameters. Because the center frequency obtained by VMD does not need to be calculated like other features, a feature extraction method based on GA-VMD and center frequency is proposed and applied to bearing fault diagnosis. Compared with other methods, the method proposed in this paper has clear physical significance, and it is simpler and has higher recognition rate. After the feature extraction, we utilize K-Nearest Neighbor (KNN) [32] to classify all kinds of fault bearing signals, and both the simulated signal and the actual bearing signal experimental results show the effectiveness of the feature extraction method proposed in this paper.

The rest of this paper is structured as follows. Section 2 proposes GA-VMD algorithm and introduces the specific steps of GA-VMD algorithm. Section 3 introduces the main steps of the proposed fault feature extraction method. Section 4 carries out the simulation signal experiment and compares the GA-VMD algorithm and PSO-VMD algorithm. Section 5 carries out the experiments of bearing signal extraction and KNN classification based on center frequency and envelope entropy, respectively. Section 6 gives conclusion of this paper.

2. Basic Principles

2.1. Variational Mode Decomposition. Variational mode decomposition (VMD) is an adaptive signal decomposition algorithm. It can decompose a signal into multiple components, and its essence and core idea is the construction and solution of the variational problems. The solution process is as follows:

Firstly, set the variational model:

$$\max_{\{u_k\},\{\omega_k\}} \left\{ \sum_{k=1}^{K} \partial_t \left[\left(\delta(t) + \frac{j}{\pi t} \right) * u_k(t) \right] e_2^{-j\omega_k t 2} \right\}, \tag{1}$$

$$\text{s.t} \sum_{k=1}^{K} u_k = f, \tag{2}$$

where ∂_t is partial derivative operation, $\delta(t)$ is the Dirichlet distribution function, $*$ represents convolution, $\{u_k\} = \{u_1, u_2, u_3, \ldots, u_K\}$ represents K IMFs obtained by VMD, $\{\omega_k\} = \{\omega_1, \omega_2, \omega_3, \ldots, \omega_K\}$ represents the center frequency of each IMF, f represents the original signal, and K is the number of IMFs.

Then, (1) is transformed into an unconstrained problem by using penalty factor and multiplication operator; the augmented Lagrange function is obtained as follows:

$$L(\{u_k\}, \{\omega_k\}, \lambda) = \alpha \sum_{k=1}^{K} \delta_t \left[\left(\delta(t) + \frac{j}{\pi t} \right) * u_k(t) \right] e^{-j\omega_k t 2} + f(t) - \sum_{k=1}^{K} u_k(t) + \lambda(t), f(t) - \sum_{k=1}^{K} u_k(t), \tag{3}$$

where λ is the Lagrange constant, and α is the penalty factor.

Lastly, for the sake of solving the optimal solution of the variational problem, it is necessary to update variable by alternating direction multiplier of method (ADMM). Updated after $n+1$ cycles, update the formulas for $\widehat{u}_k^{n+1}$, ω_k^{n+1}, and $\widehat{\lambda}^{n+1}$ as follows:

$$\frac{\hat{f}(\omega) - \sum_{i<k} \hat{u}_i^{n+1}(\omega) - \sum_{i>k} \hat{u}_i^{n}(\omega) + x\widehat{\lambda}^{n}(\omega)/2}{1 + 2\alpha(\omega - \omega_k^n)^2} \longrightarrow \widehat{u}_k^{n+1}(\omega),$$

$$\frac{\int_0^\infty \omega \left| \widehat{u}_k^{n+1}(\omega) \right|^2 d\omega}{\int_0^\infty \left| \widehat{u}_k^{n+1}(\omega) \right|^2 d\omega} \longrightarrow \omega_k^{n+1},$$

$$\widehat{\lambda}^{n}(\omega) + \tau \left(\widehat{f}(\omega) - \sum_{k} \widehat{u}_k^{n+1}(\omega) \right) \longrightarrow \widehat{\lambda}^{n+1}(\omega), \tag{4}$$

where τ is the noise tolerance, and $\widehat{u}_i^{n+1}(\omega)$, $\widehat{u}_i^{n}(\omega)$, $\widehat{f}(\omega)$ and $\widehat{\lambda}^{n}(\omega)$ correspond to the Fourier transform of $u_i^{n+1}(\omega)$, $u_i^{n+1}(\omega)$, $f(\omega)$ and $\lambda^n(\omega)$, respectively.

The main iterative solution process of VMD algorithm is as follows:

(1) Initialize $\{\widehat{u}_k^1\}$, $\{\omega_k^1\}$, $\left\{\widehat{\lambda}^1\right\}$

(2) $n = n + 1$, enter the cycle, where n is the number of iterations

(3) Update u_k, ω_k, λ

(4) Repeat steps (2) through (5) until the iteration stop condition is satisfied:

$$\sum_k \frac{\left\|\hat{u}_k^{n+1} - \hat{u}_k^n\right\|_2^2}{\left\|\hat{u}_k^n\right\|_2^2} < \varepsilon, \tag{5}$$

where ε is a constant and $\varepsilon > 0$.

2.2. Optimization of VMD by Genetic Algorithm. As a signal decomposition algorithm, the variational modal decomposition (VMD) algorithm is greatly affected by the number of modal components and penalty factors, so it is necessary to use the optimization algorithm to optimize the parameters. Compared with the particle swarm optimization (PSO) algorithm, the genetic algorithm (GA) has higher global performance and a more mature convergence analysis method. The optimal parameters of VMD algorithm are searched by optimization algorithm. The algorithm steps of GA-VMD are shown in Figure 1, and the algorithm steps of GA-VMD are as follows:

(1) The parameters of GA algorithm are determined, and the optimization objective function can be expressed as

$$C = \min \sum_{i=1}^{K} \frac{E_i}{K}. \tag{6}$$

Constraints can be expressed as

$$\text{s.t.} \begin{cases} K_{\min} \le K_i \le K_{\max} \\ a_{\min} \le a_i \le a_{\max} \\ K \in N+,\ a \in N+ \end{cases}, \tag{7}$$

where K is the optimal number of IMFs, i is the IMF serial number ($i = 1,2,3, ...$) obtained from the decomposition of the original signal, E_i represents the envelope entropy of the i-th IMF, C is the objective function, a_i is the penalty factor of the i-th IMF, K_i is the optimal number of IMF for the i-th IMF, and N is natural number.

(2) Initialize the population, namely, VMD parameter [K, α].

(3) Input the population into VMD to obtain the IMFs, calculate the average envelope entropy of all IMFs as the fitness function, and save the minimum average envelope entropy and its corresponding VMD parameters [K, α], and the envelope entropy can be expressed as

$$\begin{cases} P_{i,j} = \dfrac{a_i(j)}{\sum_{j=1}^{N} a_i(j)} \\ \\ E_i = -\sum_{j=1}^{N} P_{i,j} lg p_{i,j} \end{cases}, \tag{8}$$

where $a_i(j)$ is the envelope signal obtained from the signal $\mathrm{IMF}_i(j)$ after Hilbert mediation, and $P_{i,j}$ is the normalized form of the signal $a_i(j)$.

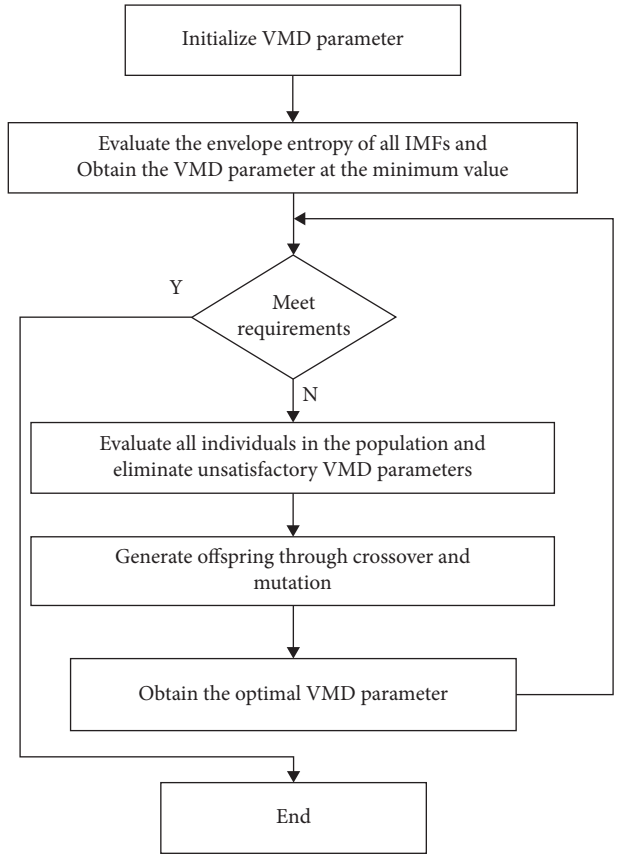

Figure 1: The algorithm steps of GA-VMD.

(4) Evaluate the fitness of all individuals in the population, that is, the parameter combination, and eliminate unsatisfactory individuals.

(5) According to the principle that the higher the fitness is, the greater the selection probability is, two individuals are selected from the population as the parent and mother, and the offspring are generated through binary crossover and mutation;

(6) Repeat steps (4) and (5) and update the population;

(7) Cycle steps (3) ~ (6) until the maximum number of iterations is completed;

(8) The minimum value of the local minimum average envelope entropy in each iteration obtained in step (7) is selected as the global minimum value of this optimization, and its corresponding parameter combination [K, α] is the best parameter combination obtained in this optimization.

3. Fault Feature Extraction Method

The bearing fault feature extraction flow chart is shown in Figure 2, and the specific steps are as follows.

(1) The bearing signals under four different states are obtained, including normal signal, inner ring fault signal, outer ring fault signal, and rolling element fault signal.

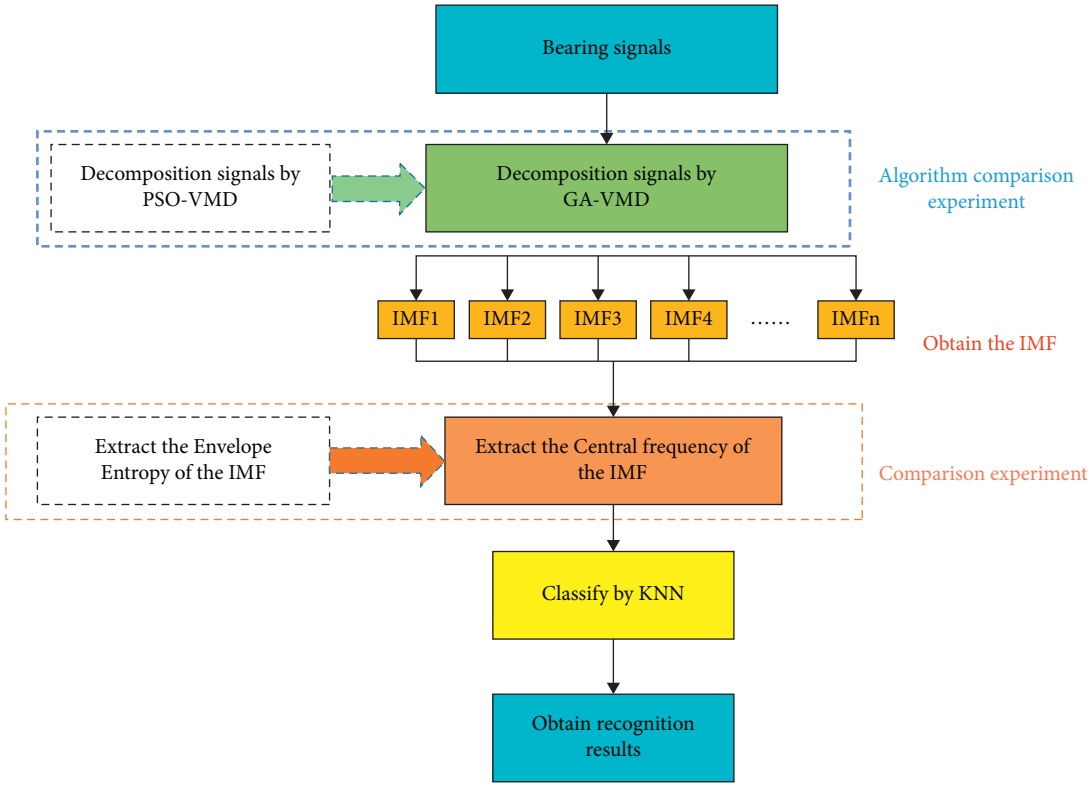

Figure 2: Bearing fault feature extraction flow chart.

(2) GA-VMD algorithm is used to carry out signal adaptive decomposition of the four types of bearing signals, and the IMF combinations are obtained. The effectiveness of GA-VMD algorithm is convinced through simulation signal analysis in Section 4.

(3) The central frequency of bearing signal IMF is extracted, and a comparison experiment with the envelope entropy is carried out.

(4) Recognition results of bearing signals are obtained through KNN.

4. Simulation Signal Analysis

In order to verify the effectiveness of GA-VMD algorithm, the VMD decomposition results based on particle swarm optimization algorithm are compared with the proposed method in this paper. Set up a set of simulation signals for analysis, and its specific expression is

$$X = x_1 + x_2 + x_3 + x_4,$$
$$\begin{cases} x_1 = 10\cos\left(2\pi f_1 t + 3.5\right) \\ x_2 = 10\cos\left(2\pi f_2 t + 2.0\right) \\ x_3 = 10\cos\left(2\pi f_3 t + 1.5\right) \\ x_4 = 10\cos\left(2\pi f_4 t + 1.0\right) \end{cases}, \quad (9)$$

where X is the original signal, x_1, x_2, x_3, x_4 are the subsignals, f_1, f_2, f_3, f_4 are the subfrequencies of x_1, x_2, x_3, x_4, and their values are, respectively, 170 Hz, 120 Hz, 50 Hz, and 10 Hz.

Set the number of analysis points N as 1024 and the sampling frequency f_s as 1024 kHz. Figure 3 shows the time-domain waveform of the simulation signal and its original component.

The root mean square error is used to calculate the amplitude difference between the original component signal and the decomposed component signal to verify the decomposition performance of the two algorithms. The root mean square error calculation formula is

$$\mathrm{RMSE} = \sqrt{\frac{\sum_{i=1}^{n}\left[\widehat{f}\left(t_i\right) - f\left(t_i\right)\right]^2}{n}}, \quad (10)$$

where n is the number of observations, $\widehat{f}\left(t_i\right)$ is the original component signal, and $f\left(t_i\right)$ is decomposed component signal. The root mean square error reflects the difference of signal amplitude between the decomposed signal and the original signal component. The smaller the RMSE value is, the better the decomposition effect is.

The VMD algorithm based on genetic algorithm (GA-VMD) and the parameter optimization VMD algorithm based on particle swarm optimization (PSO-VMD) are used to decompose the simulation signal. The genetic algorithm parameters are set as follows: the initial population is 20, the number of iterations is 100, the crossover probability is 0.8, and the mutation probability is 0.4. The specific parameters of Particle swarm optimization are as follows: the inertia weight W is 1, the acceleration factors C1 and C2 are 1.5, the maximum optimization speed of K value is 1, the minimum optimization speed is −1, and the optimization range is 3 to

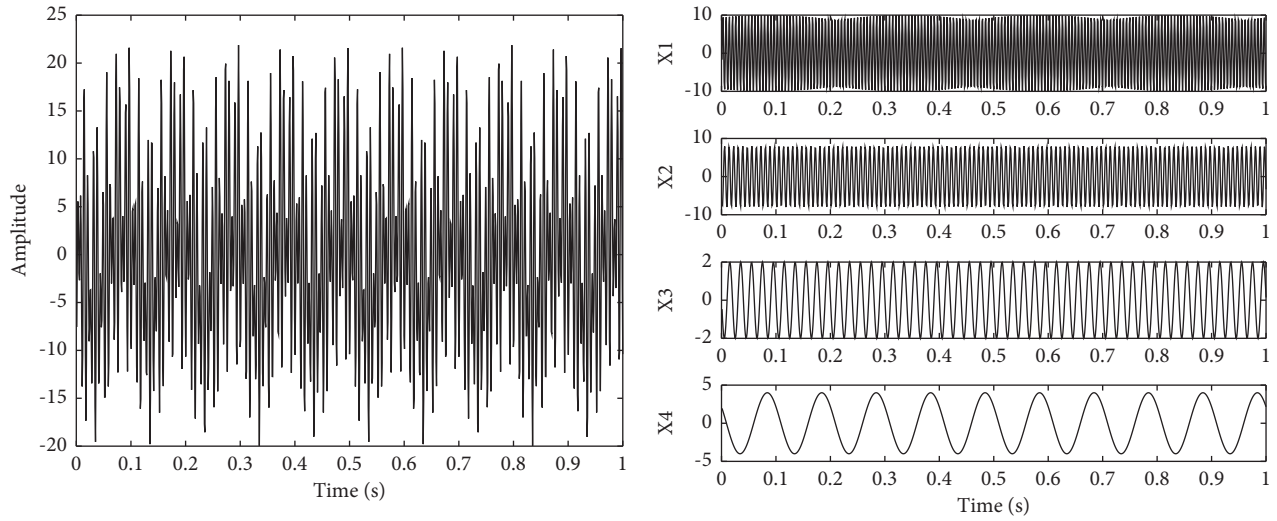

(a) (b)

Figure 3: The time-domain waveform of the simulation signal and its original component. (a) The simulation signal. (b) The original component.

5. The maximum optimization speed of α value is 2000, the minimum optimization speed is 200, and the optimization range is from 200 to 2000. The optimal input parameters obtained by GA-VMD and PSO-VMD search are $(K, a) = [4, 984]$ and $[4, 1264]$, respectively. GA-VMD and PSO-VMD decomposition results are shown in Figures 4 and 5.

According to Figures 4 and 5, IMF1 corresponds to the original signal component x_1, IMF2 to the original signal component x_2, IMF3 to the original signal component x_3, and IMF4 to the original signal component x_4. Since there are two parameters in the parameter combination, modal component K and penalty factor α, to prove the influence of the two parameters on the decomposition results, the values of K and α are changed, respectively, for VMD decomposition. The four groups of VMD parameter combinations determined manually are as follows: when the value of α change and the value of K remain unchanged, determine the parameter combination $(K, a) = [4, 500]$, $[4, 1029]$, *an d* $[4, 1500]$; when the value of K changes and the value of α remain unchanged, determine the parameter combination $(K, a) = [5, 984]$;

To further compare the effectiveness of the two algorithms and manual parameter setting-VMD, the root mean square error of the two optimization algorithms and manual parameter setting-VMD are shown in Table 1.

It can be seen from Table 1 that the root mean square error of the optimal result of GA-VMD is 0.002 lower than that of PSO-VMD, and the IMF decomposed by GA-VMD is closer to the original signal component. In addition, The root mean square error of GA-VMD is lower than that of Manual parameter setting-VMD. Therefore, GA-VMD is used to analyze the bearing fault signal in this paper.

5. Bearing Signal Feature Extraction

5.1. Bearing Signals. Bearing signal feature extraction experiment adopts bearing data provided by the laboratory of Case Western Reserve University [33]. The diameter of rolling bearing failure is 0.1778 mm, and the speed is 1730r/min. Normal signal and the sampling frequency of the signal, which include acceleration data of inner ring fault, outer ring fault, and rolling element fault obtained from the rolling bearing fault, are 12 kHz. There are 100 samples for each type of bearing signal, and each sample contains 1200 sampling points. The time-domain waveform of rolling bearing signals under four states (one sample) is shown in Figure 6.

5.2. Bearing Signal Decomposition. The optimal number of IMF components K of the four bearing signals decomposed by GA-VMD algorithm is 9, and the penalty factors α are 12040, 15480, 9880, and 15560, respectively. The decomposition results of the four bearing signals obtained are shown in Figure 7.

In order to further verify the effectiveness of GA-VMD algorithm, comparative experiments with PSO-VMD algorithm are carried out. The bearing signal is decomposed by PSO-VMD to obtain the corresponding IMF, and then the root mean square error of the measured signal by the two optimization algorithms is shown in Table 2.

It can be seen from Table 2 that, for each bearing signal, the root mean square error of the optimization result of GA-VMD is lower than that of PSO-VMD, especially normal signal and rolling element fault signal; for normal signal, the root mean square error of GA-VMD is about 0.01 lower than

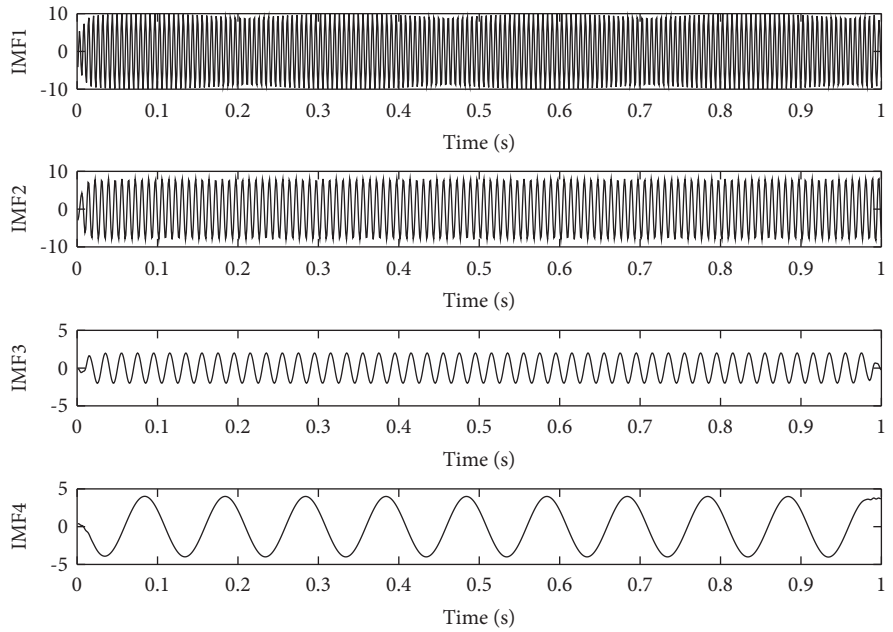

Figure 4: GA-VMD decomposition result.

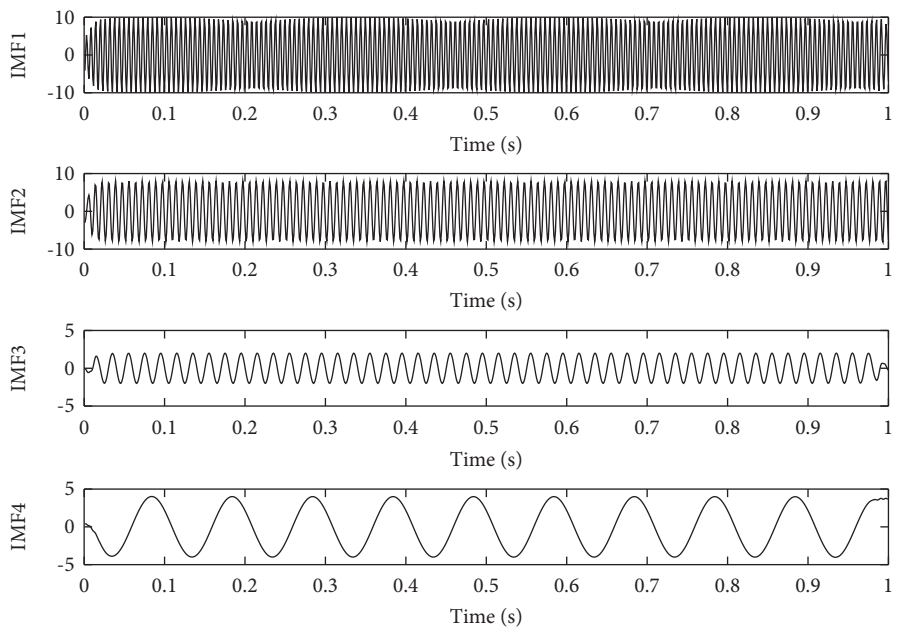

Figure 5: PSO-VMD decomposition result.

Table 1: The root mean square error of the two optimization algorithms and manual parameter setting-VMD.

	GA-VMD	PSO-VMD	Manual parameter setting-VMD			
$[K, \alpha]$	[4, 984]	[4, 1264]	[4, 500]	[4, 1185]	[4, 1500]	[5, 984]
RMSE	0.2104	0.2143	1.0001	0.2131	0.6326	0.2568

that of PSO-VMD; for rolling element fault signal, the root mean square error of GA-VMD is about 0.0176 lower than that of PSO-VMD. Therefore, compared with PSO-VMD, GA-VMD has better optimization results.

5.3. Feature Extraction of Bearing Signals. The characteristics of center frequency and envelope entropy of IMF of four kinds of bearing signals are extracted. The characteristic distribution of center frequency and envelope entropy of

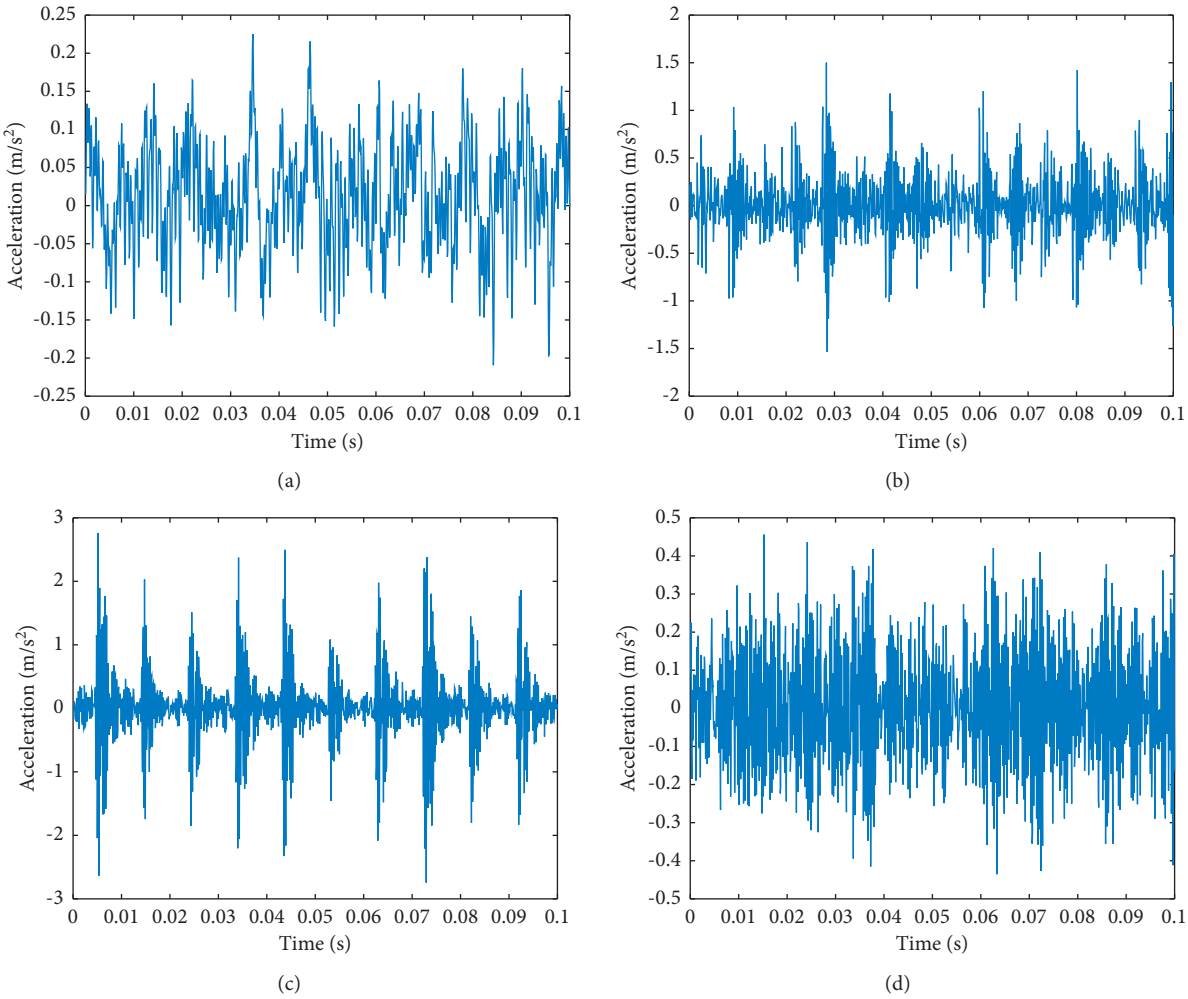

Figure 6: The time-domain waveform of rolling bearing signals under four states. (a) Normal. (b) Inner ring fault. (c) Outer ring fault. (d) Rolling element fault.

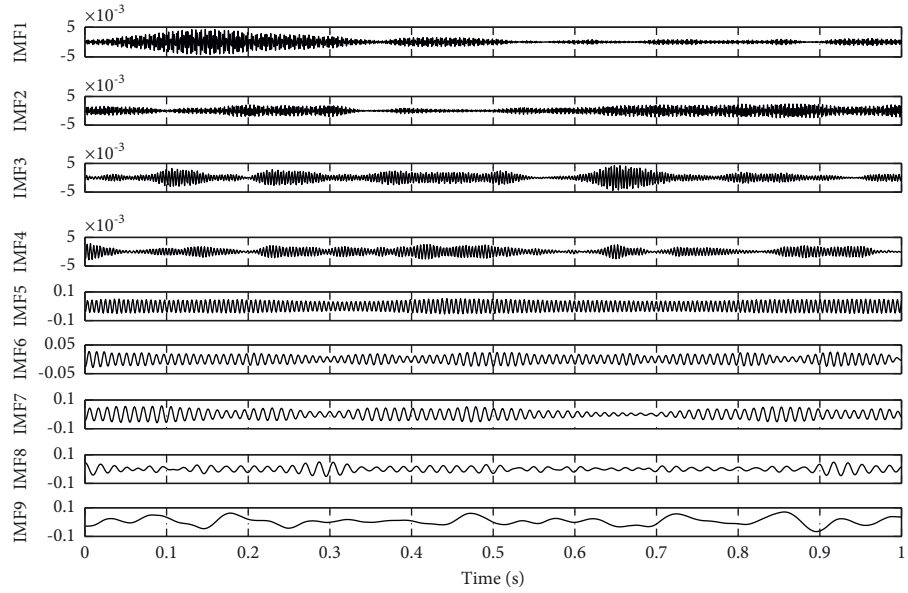

Figure 7: Continued.

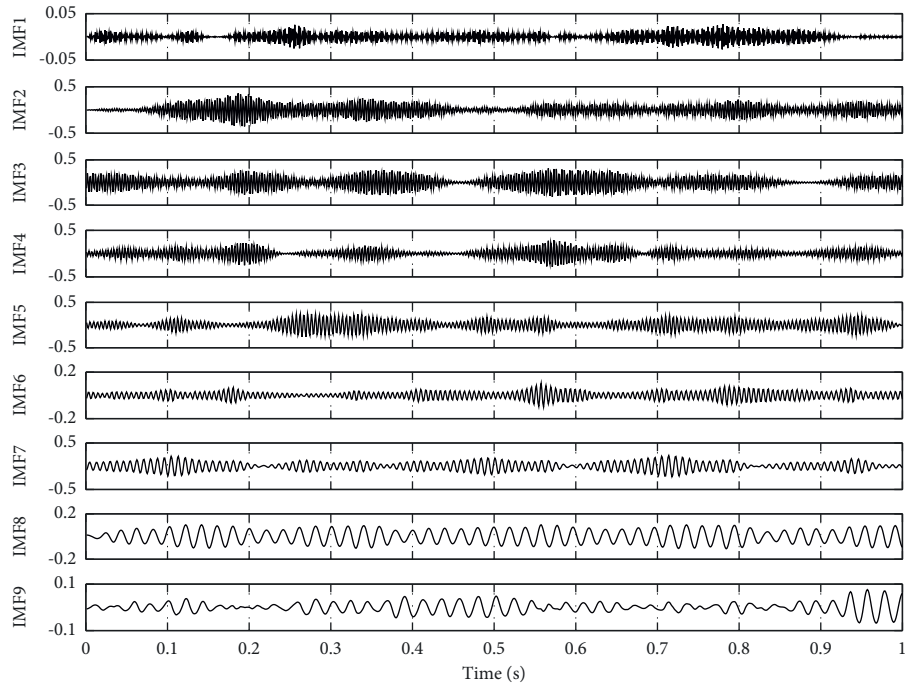

(b)

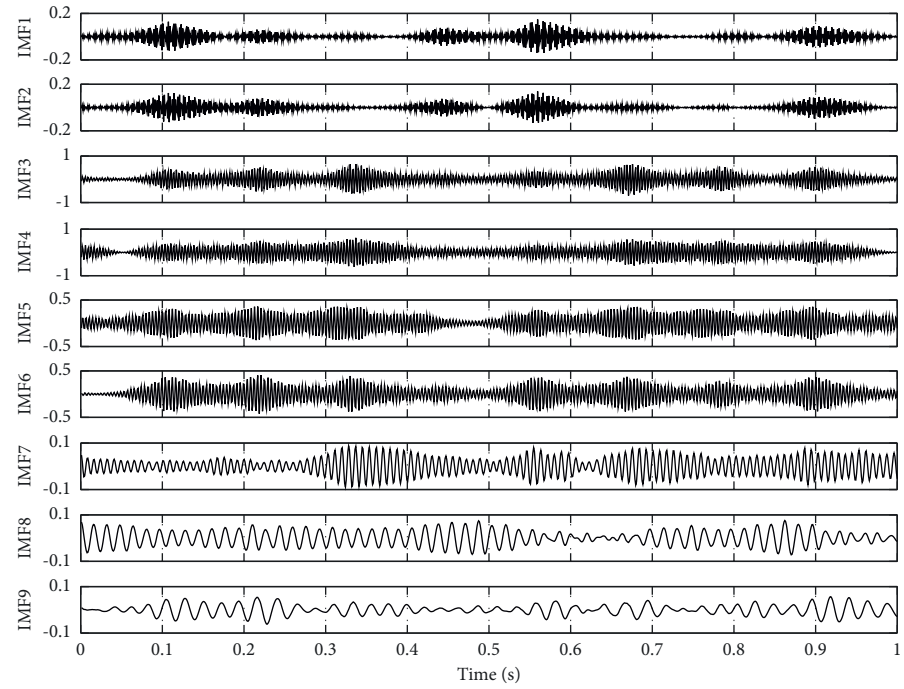

(c)

Figure 7: Continued.

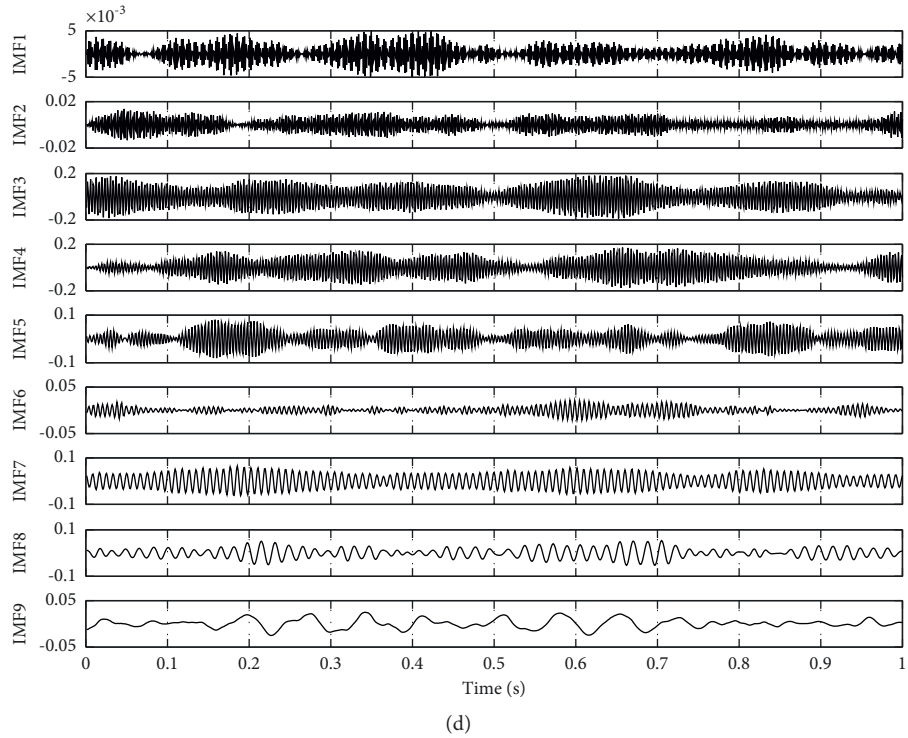

(d)

Figure 7: The decomposition results of the four bearing signals. (a) Normal. (b) Inner ring fault. (c) Outer ring fault. (d) Rolling element fault.

Table 2: The root mean square error of the measured signal by the two optimization algorithms.

Bearing signal	GA-VMD		PSO-VMD	
	$[K, \alpha]$	RMSE	$[K, \alpha]$	RMSE
Normal	[4, 12040]	0.2204	[4, 13500]	0.2303
Inner ring fault	[4, 15480]	0.1317	[4,18840]	0.1332
Outer ring fault	[4, 9880]	0.0694	[4,1274]	0.0821
Rolling element fault	[4, 15560]	0.1081	[4,1760]	0.1257

IMF of four kinds of bearing signals are shown in Figure 8 and 9.

It can be seen from Figures 8 and 9 that the envelope entropy distribution in each IMF of the four kinds of bearing signals is chaotic, and there are many overlaps, while the center frequency distribution of each mode of the four types of bearing signals is more regular, and the overlaps are significantly reduced; the center frequency values of inner ring fault signal, outer ring fault signal, and rolling element fault in IMF4 and IMF7 are very close, while there are obvious differences from the center frequency of normal signal; the envelope entropy of outer ring fault signals in IMF4 and IMF5 is lower than that of the other three kinds of signals; the center frequency of normal signals in IMF7 is almost at the same level, and the frequency range of the center frequency of other three types of bearing signals also has obvious differences; compared with enveloping entropy, extracting center frequency features is more beneficial to distinguish four kinds of bearing signals.

5.4. Classification of Bearing Signals

5.4.1. Single Feature Classification. For purpose of further identifying the features, KNN classifier is used to classify the signals. The center frequency and envelope entropy of a single IMF in 200 sample signals in each of the four states are classified as characteristic parameters.

KNN is one of the most basic and simplest machine learning algorithms. KNN is classified by measuring the distance between different eigenvalues. Its core idea is as follows: a sample is most similar to the K samples in the dataset. If most of the K samples belong to category A, the sample also belongs to category A. The method only determines the category of the samples to be divided according to the category of the nearest one or several samples.

In KNN, the number of neighbors K is 1. Besides, in this experiment, for each type of bearing signal, 200 samples are randomly selected; the first 50 sample signals are used as training samples, while the other 150 sample signals are used as test samples. The characteristic classification results of the

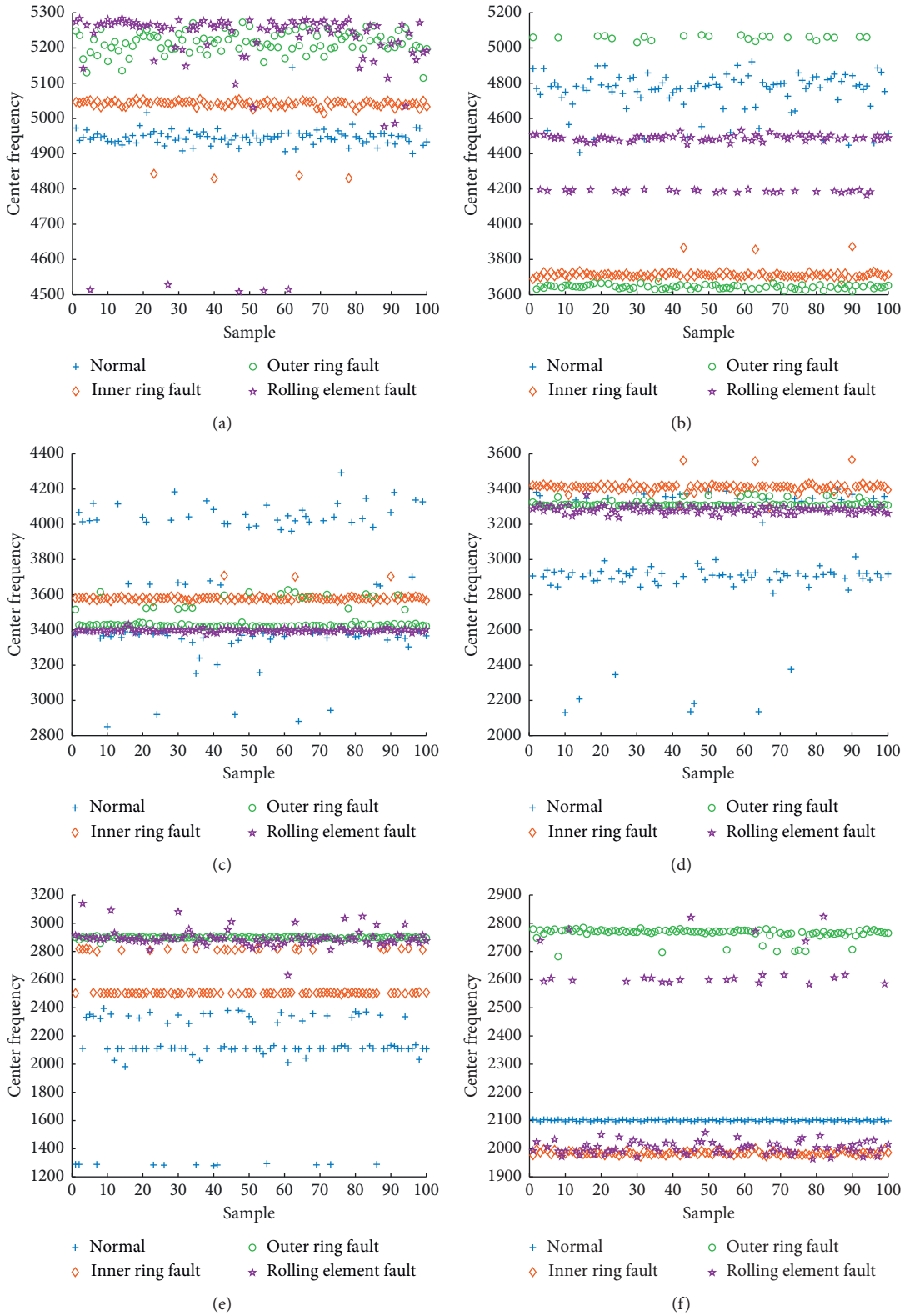

Figure 8: Continued.

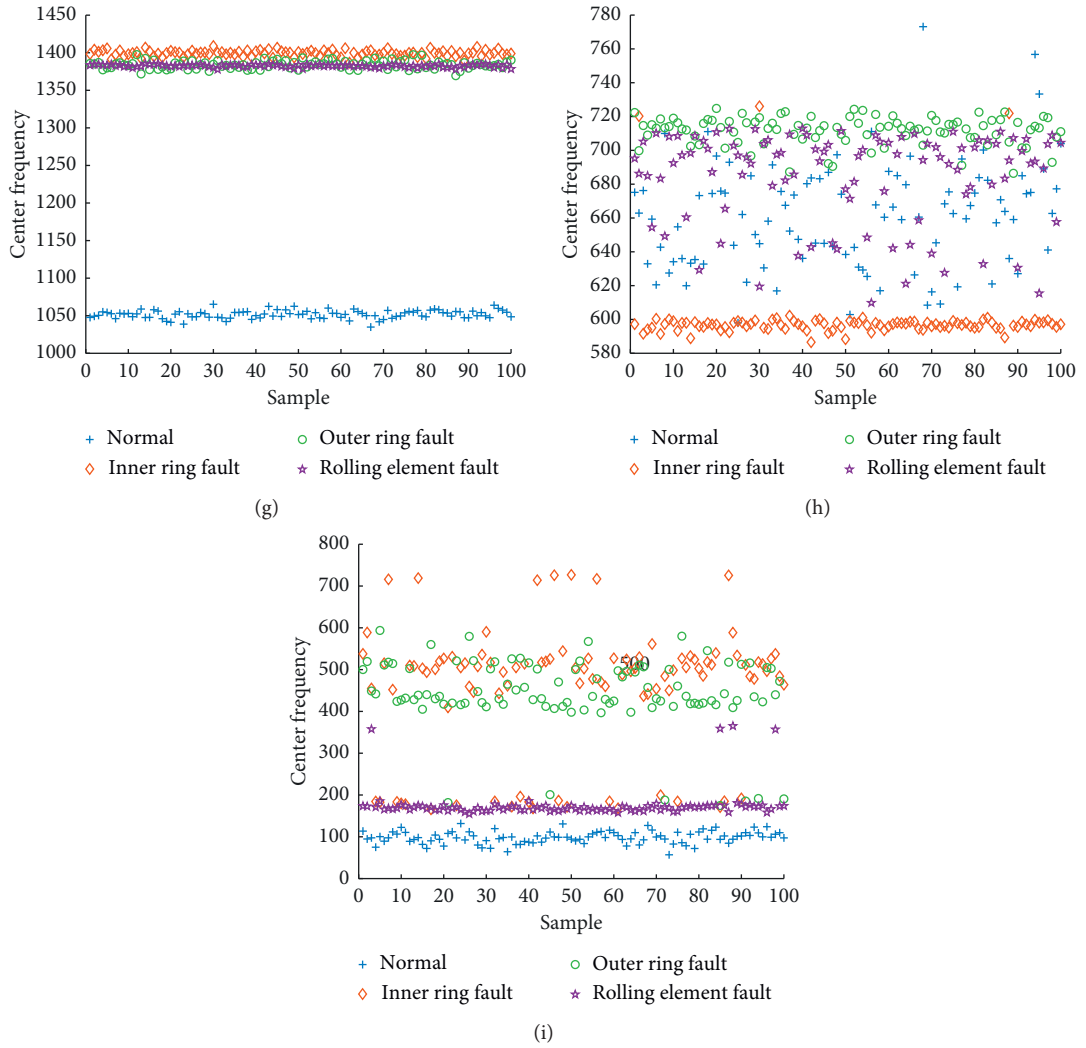

Figure 8: The characteristic distribution of center frequency of IMF of four kinds of bearing signals. (a) IMF1. (b) IMF2. (c) IMF3. (d) IMF4. (e) IMF5. (f) IMF6 (g). IMF7 (h). IMF8. (i) IMF9.

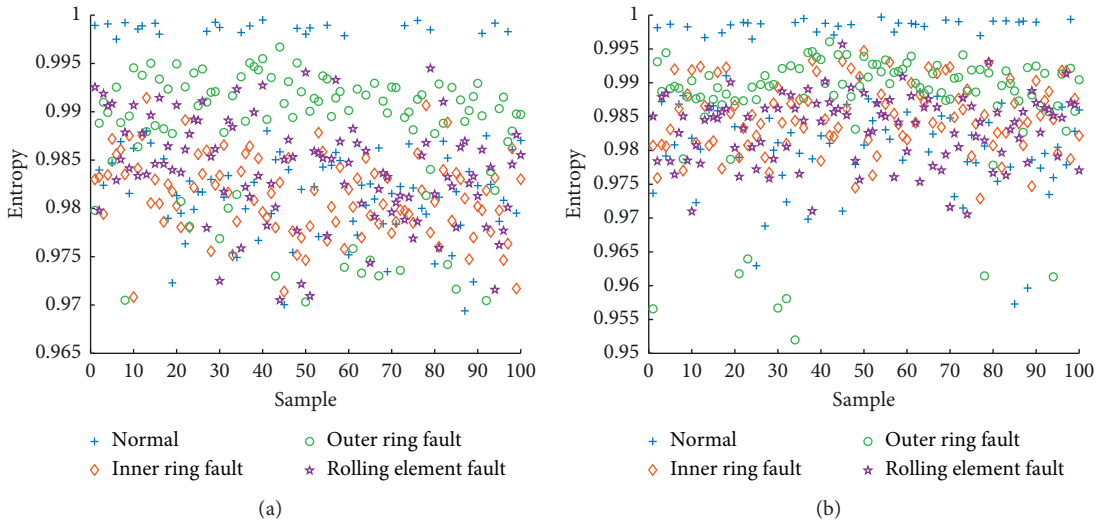

Figure 9: Continued.

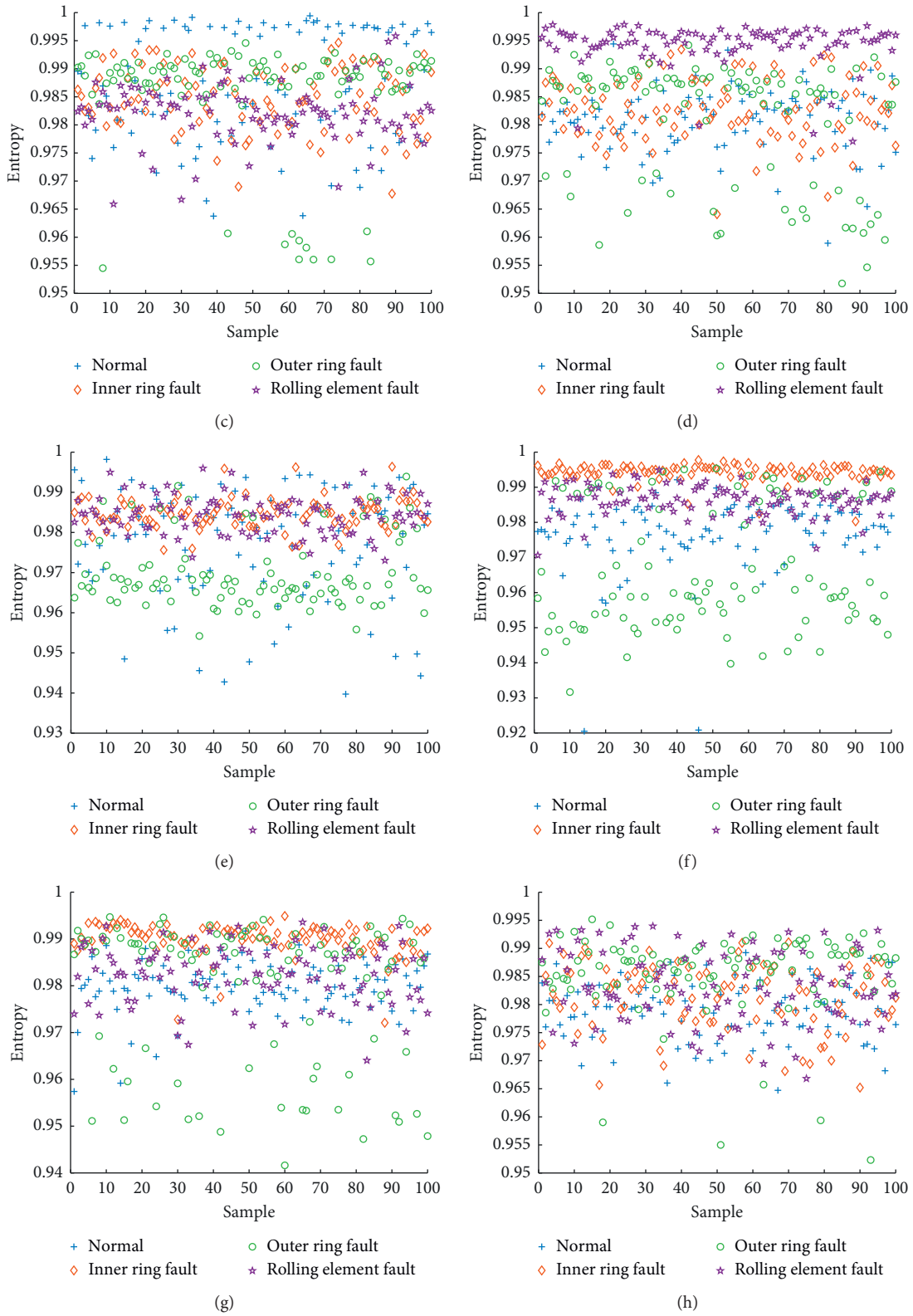

Figure 9: Continued.

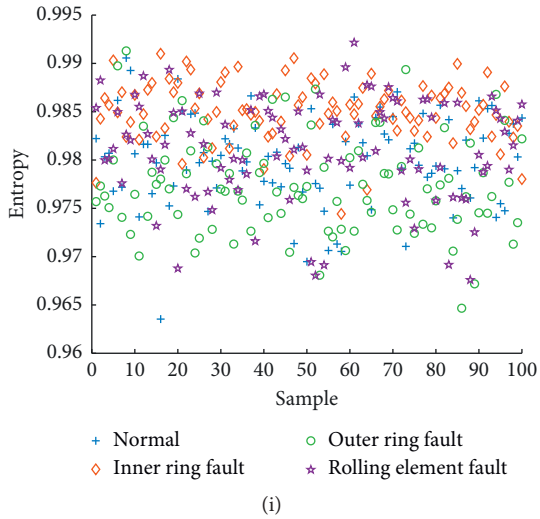

Figure 9: The characteristic distribution of envelope entropy of IMF of four kinds of bearing signals. (a) IMF1. (b) IMF2. (c) IMF3. (d) IMF4. (e) IMF5. (f) IMF6 (g). IMF7 (h). IMF8. (i) IMF9.

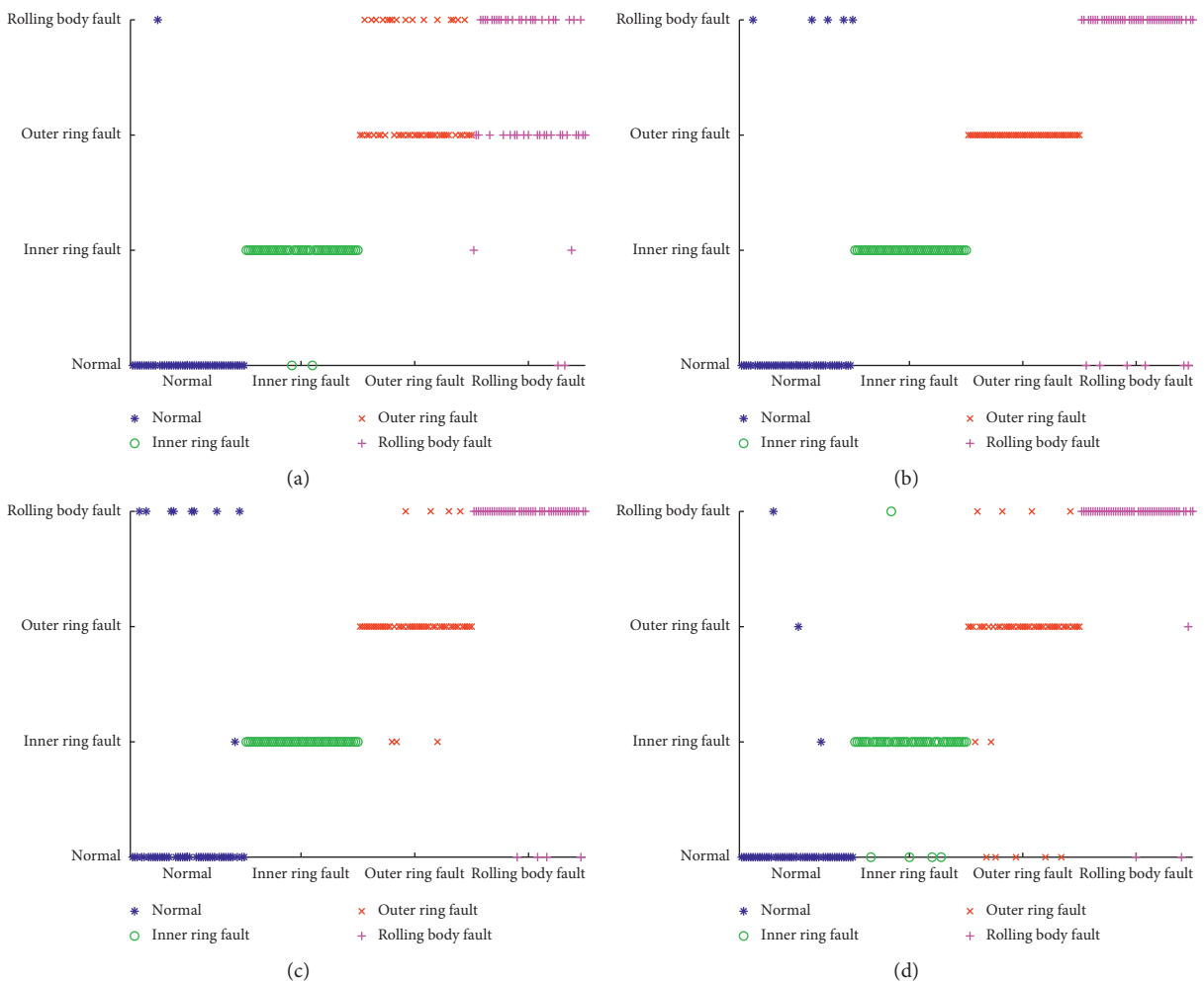

Figure 10: Continued.

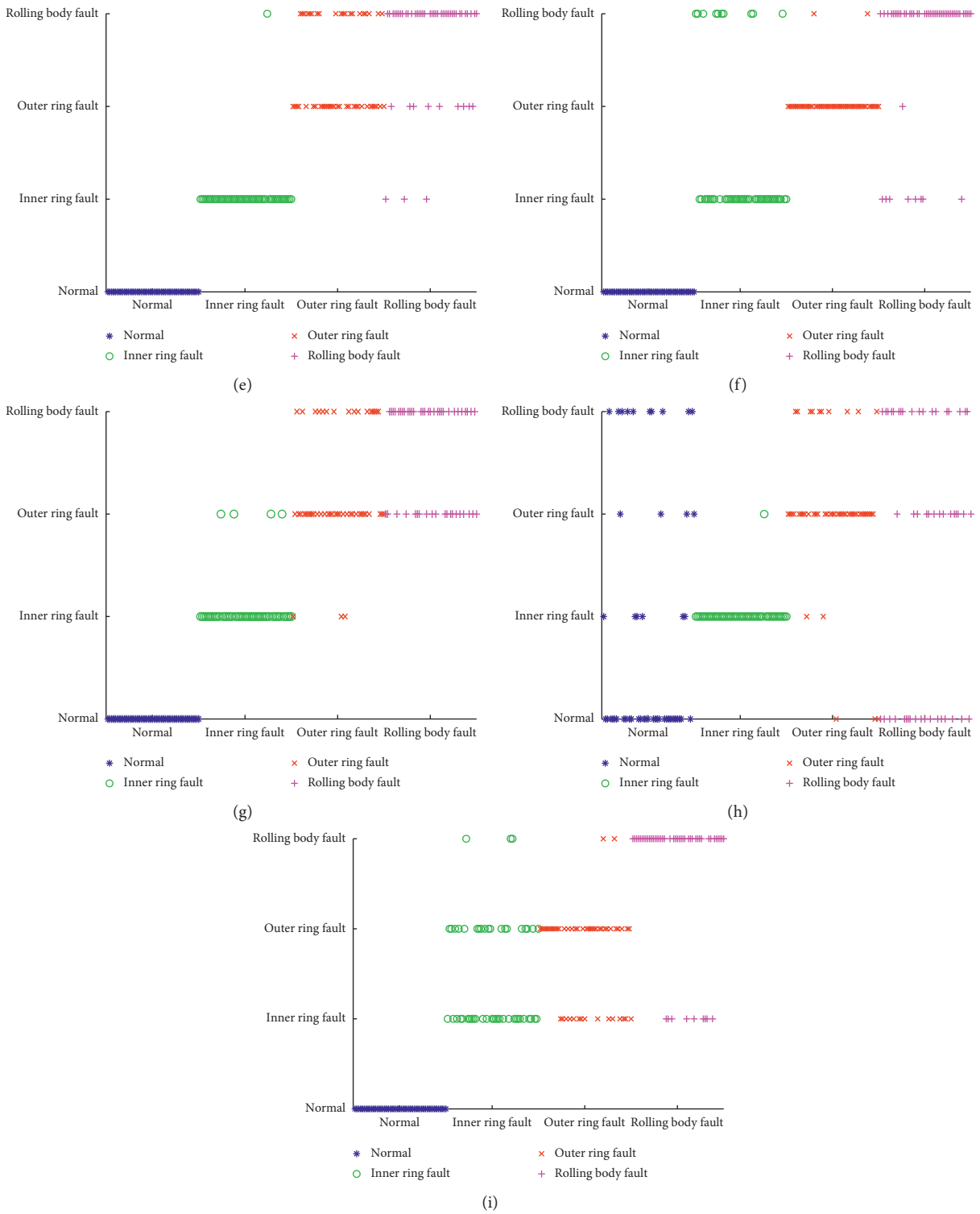

Figure 10: The characteristic classification results of the center frequency of each IMF. (a) IMF1. (b) IMF2. (c) IMF3. (d) IMF4. (e) IMF5. (f) IMF6 (g). IMF7 (h). IMF8. (i) IMF9.

Figure 11: Continued.

FIGURE 11: The characteristic classification results of the envelope entropy of each IMF. (a) IMF1. (b) IMF2. (c) IMF3. (d) IMF4. (e) IMF5. (f) IMF6 (g). IMF7 (h). IMF8. (i) IMF9.

center frequency and envelope entropy of each IMF are shown in Figures 10 and 11.

It can be seen from Figures 10 and 11 that, compared with the envelope entropy feature, under the same mode, fewer samples are identified incorrectly by using the method characterized by center frequency; for the center frequencies of different modes, IMF2 has the best result of feature classification. Classification recognition rates of single IMF component center frequency and envelope entropy are shown in Table 3 and 4 respectively.

It can be seen from Tables 3 and 4 that the center frequency feature extraction and recognition effect of a single IMF component is better than that of the single component feature extraction and recognition of IMF component envelope entropy; the average recognition rate of envelope entropy feature of single IMF component is generally lower than 60%, some even lower than 40%, and the maximum recognition rate is 61%; the recognition effect is poor, so it is impossible to identify and diagnose the four bearing signals; except for a few components, the accuracy of extraction and classification of central frequency features of most IMF components reached more than 75%, and the accuracy of IMF2 component even reached 94.5%; in the recognition of normal signals, the recognition accuracy of center frequency of IMF5, IMF6, IMF7, and IMF9 components all reached 100%; the recognition rate of IMF2 and IMF3 component center frequency in inner ring fault recognition is also 100%.

5.4.2. Multifeature Classification. Aiming to improve the signal recognition rate, a multicomponent feature recognition method is adopted, that is, the method of simultaneously recognizing the center frequency or envelope entropy of multiple IMF components, to classify and recognize the four bearing signals.

KNN classifier is used to extract and classify the component features of the center frequency and envelope entropy of the four kinds of bearing signals. Classification

Table 3: Classification recognition rates of single IMF component center frequency.

IMF	Classification and recognition accuracy (%)				
	Normal	Inner ring fault	Outer ring fault	Rolling element fault	Mean
IMF1	98	96	68	50	78
IMF2	90	100	100	88	94.5
IMF3	82	100	86	92	90
IMF4	94	90	78	94	89
IMF5	100	98	60	76	83.5
IMF6	100	80	96	82	89.5
IMF7	100	92	62	60	78.5
IMF8	60	98	70	36	66
IMF9	100	56	66	82	76

Table 4: **C**lassification recognition rates of single IMF component envelope entropy.

IMF	Classification and recognition accuracy (%)				
	Normal	Inner ring fault	Outer ring fault	Rolling element fault	Mean
IMF1	28	50	76	34	47
IMF2	44	44	98	40	56.5
IMF3	28	42	56	22	37
IMF4	32	40	60	42	43.5
IMF5	60	28	40	60	47
IMF6	90	54	36	64	61
IMF7	56	38	46	90	57.5
IMF8	40	70	38	44	48
IMF9	22	48	26	33	38

Table 5: Classification recognition rates of center frequency.

IMF	Classification and recognition accuracy (%)				
	Normal	Inner ring fault	Outer ring fault	Rolling element fault	Mean
$IMF_{1\sim2}$	100	100	100	94	98.5
$IMF_{1\sim3}$	100	100	100	94	98.5
$IMF_{1\sim4}$	100	100	100	100	100
$IMF_{1\sim5}$	100	100	100	100	100
$IMF_{1\sim6}$	100	100	100	100	100
$IMF_{1\sim7}$	100	100	100	100	100
$IMF_{1\sim8}$	100	100	100	100	100
$IMF_{1\sim9}$	100	100	100	100	100

Table 6: Classification recognition rates of envelope entropy.

IMF	Classification and recognition accuracy (%)				
	Normal	Inner ring fault	Outer ring fault	Rolling element fault	Mean
$IMF_{1\sim2}$	40	62	100	50	63.0
$IMF_{1\sim3}$	40	50	100	40	57.5
$IMF_{1\sim4}$	38	54	100	46	59.5
$IMF_{1\sim5}$	56	80	100	66	75.5
$IMF_{1\sim6}$	84	98	100	96	94.5
$IMF_{1\sim7}$	86	100	100	98	96.0
$IMF_{1\sim8}$	92	98	100	96	96.5
$IMF_{1\sim9}$	96	100	100	98	98.5

recognition rates of center frequency and envelope entropy are shown in Tables 5 and 6, where $IMF_{1\text{-}2}$ means to simultaneously identify the features of IMF component 1 and 2 signals, $IMF_{1\sim3}$ means to simultaneously identify the features of IMF component 1, 2 and 3 signals, and so on.

It can be seen from Tables 4 and 5 that, under the same number of components, the classification effect of multicomponent central frequency feature extraction is significantly better than that of multicomponent envelope entropy feature extraction; when the number of IMFs is greater than 2, the average recognition rate of envelope entropy feature extraction increases with the increase of the number of components, up to 98.5%; the average recognition rate of multicomponent center frequency feature extraction is not less than 98.5%, which is higher than the highest value of recognition rate of envelope entropy feature extraction; when the number of components is 9, the envelops entropy feature extraction effect is optimal, and the average recognition rate is 98.5%; when the number of components is 4, the recognition accuracy of multifeature center frequency extraction has reached 100%; therefore, compared with feature extraction based on envelope entropy, feature extraction based on center frequency can achieve higher recognition rate in the case of a small number of components and can realize effective recognition of bearing faults.

6. Conclusion

In this paper, a bearing fault feature extraction method based on GA-VMD and center frequency is proposed, and the feasibility of the proposed method is verified by feature extraction and classification recognition experiments on four kinds of measured bearing signals. The main conclusions are as follows:

(1) Compared with PSO-VMD algorithm, the root mean square error of GA-VMD algorithm is smaller, and the decomposed IMF is closer to the corresponding signal component

(2) For single feature extraction method, the highest recognition rate of feature extraction method based on center frequency is 94.5%, which is 33.5% higher than that of feature extraction method based on envelope entropy

(3) Compared with the single feature extraction method, the average recognition rate of multifeature extraction method is 17% (center frequency) and 32% (envelope entropy) higher than that of single feature extraction method; compared with the multifeature center frequency extraction method, the average recognition rate of multifeature center frequency feature extraction method is 19.5% higher than that of multifeature envelope entropy extraction method

Data Availability

Data are available upon request to the authors.

Conflicts of Interest

The authors declare that they have no conflicts of interest.

References

[1] L. Zhang, J. Lin, and R. Karim, "Adaptive kernel density-based anomaly detection for nonlinear systems," *Knowledge-Based Systems*, vol. 139, pp. 50–63, 2018.

[2] S. Haidong, C. Junsheng, J. Hongkai, Y. Yu, and W. Zhantao, "Enhanced deep gated recurrent unit and complex wavelet packet energy moment entropy for early fault prognosis of bearing," *Knowledge-Based Systems*, vol. 188, Article ID 105022, 2020.

[3] Y. Li, S. Wang, and Z. Deng, "Intelligent fault identification of rotary machinery using refined composite multi-scale Lempel-Ziv complexity," *Journal of Manufacturing Systems*, vol. 61, pp. 725–735, 2021.

[4] J. Zheng and H. Pan, "Use of generalized refined composite multiscale fractional dispersion entropy to diagnose the faults of rolling bearing," *Nonlinear Dynamics*, vol. 101, no. 2, pp. 1417–1440, 2020.

[5] B. Cai, H. Liu, and M. Xie, "A real-time fault diagnosis methodology of complex systems using object-oriented Bayesian networks," *Mechanical Systems and Signal Processing*, vol. 80, pp. 31–44, 2016.

[6] Y. Li, X. Wang, Z. Liu, X. Liang, and S. Si, "The entropy algorithm and its variants in the fault diagnosis of rotating machinery: a review," *IEEE Access*, vol. 6, Article ID 66723, 2018.

[7] T. Han, C. Liu, L. Wu, S. Sarkar, and D. Jiang, "An adaptive spatiotemporal feature learning approach for fault diagnosis in complex systems," *Mechanical Systems and Signal Processing*, vol. 117, pp. 170–187, 2019.

[8] T. Han, Y. Li, and M. Qian, "A hybrid generalization network for intelligent fault diagnosis of rotating machinery under unseen working conditions," *IEEE Transactions on Instrumentation and Measurement*, vol. 70, Article ID 3520011, 2021.

[9] A. Lempel and J. Ziv, "On the complexity of finite sequences," *IEEE Transactions on Information Theory*, vol. 22, no. 1, pp. 75–81, 1976.

[10] Z. Zhang, A. Verma, and A. Kusiak, "Fault analysis and condition monitoring of the wind turbine gearbox," *IEEE Transactions on Energy Conversion*, vol. 27, no. 2, pp. 526–535, 2012.

[11] A. Babloyantz and A. Destexhe, "Is the normal heart a periodic oscillator?" *Biological Cybernetics*, vol. 58, pp. 203–211, 1988.

[12] J. Zheng, J. Cheng, Y. Yang, and S. Luo, "A rolling bearing fault diagnosis method based on multi-scale fuzzy entropy and variable predictive model-based class discrimination," *Mechanism and Machine Theory*, vol. 78, pp. 187–200, 2014.

[13] Y. Li, X. Liang, Y. Wei, and X. Wang, "A method based on refined composite multi-scale symbolic dynamic entropy and ISVM-BT for rotating machinery fault diagnosis," *Neurocomputing*, vol. 315, pp. 246–260, 2018.

[14] Y. Li, S. Jiao, and X. Gao, "A novel signal feature extraction technology based on empirical wavelet transform and reverse dispersion entropy," *Defence Technology*, vol. 17, no. 5, pp. 1625–1635, 2021.

[15] S. Jiao, B. Geng, and Y. Li, "Fluctuation-based reverse dispersion entropy and its applications to signal classification," *Applied Acoustics*, vol. 175, no. 4, Article ID 107857, 2021.

[16] N. E. Huang, Z. Shen, S. R. Long et al., "The empirical mode decomposition and the Hilbert spectrum for nonlinear and non-stationary time series analysis," *Proceedings*

Mathematical Physical & Engineering Sciences, vol. 454, no. 1971, pp. 903–995, 1998.
[17] Z. Wu and N. Huang, "Ensemble empirical mode decomposition: a noise-assisted data analysis method," *Advances in Adaptive Data Analysis*, vol. 1, no. 1, pp. 1–41, 2009.
[18] Y. Li, Y. Li, and X. Chen, "Ships' radiated noise feature extraction based on EEMD," *Journal of Vibration and Shock*, vol. 36, no. 5, pp. 114–119, 2017.
[19] Y. Li, Y. Li, X. Chen, and J. Yu, "Denoising and feature extraction algorithms using NPE combined with VMD and their applications in ship-radiated noise," *Symmetry*, vol. 9, no. 11, p. 256, 2017.
[20] Y. Li, Y. Li, and X. Chen, "Feature extraction of ship-radiated noise based on VMD and center frequency," *Journal of Vibration and Shock*, vol. 37, no. 23, pp. 213–218, 2018.
[21] K. Dragomiretskiy and D. Zosso, "Variational mode decomposition," *IEEE Transactions on Signal*, vol. 62, no. 3, pp. 531–544, 2014.
[22] J. Xia, L. Zhao, Y. Bai, and M. Yu, "Feature extraction for rolling element bearing weak fault based on MCKD and VMD," *Journal of Vibration and Shock*, vol. 36, no. 20, pp. 78–83, 2017.
[23] W. Liu, S. Cao, Z. Wang, X. Kong, and Y. Chen, "Spectral decomposition for hydrocarbon detection based on VMD and teager–kaiser energy," *IEEE Geoscience and Remote Sensing Letters*, vol. 4, pp. 1–5, 2017.
[24] L. Xie, L. Luo, Y. Li, Y. Zhang, and Y. Cao, "A traveling wave-based fault location method employing VMD-TEO for distribution network," *IEEE Transactions on Power Delivery*, vol. 35, no. 4, pp. 1987–1998, 2020.
[25] L. Cheng, W. Cheng, W. Yun, and Y. J. Zhao, "Probabilistic analyses of structural dynamic response with modified Kriging-based moving extremum framework," *Engineering Failure Analysis*, vol. 125, Article ID 105398, 2021.
[26] W. Cheng, H. Liu, S. Li, H. Li, L. An, and C. Lu, "Dynamic parametric modeling-based model updating strategy of aeroengine casings," *Chinese Journal of Aeronautics*, vol. 34, no. 12, pp. 145–157, 2021.
[27] W. Cheng, H. Li, H. Liu et al., "Enhanced network learning model with intelligent operator for the motion reliability evaluation of flexible mechanism," *Aerospace Science and Technology*, vol. 107, Article ID 106342, 2020.
[28] G. Tang and X. Wang, "Application of parameter optimization variational mode decomposition method in early fault diagnosis of rolling bearing," *Journal of Xi'an Jiaotong University*, vol. 49, no. 5, pp. 73–81, 2015.
[29] S. Mirjalili and A. Lewis, "The whale optimization algorithm," *Advances in Engineering Software*, vol. 95, pp. 51–67, 2016.
[30] S. Zhang and Y. Zhang, "Harmonic detection method based on permutation entropy and variational modal decomposition optimized by genetic algorithm," *Review of Scientific Instruments*, vol. 92, no. 2, Article ID 25118, 2021.
[31] Z. Chao and Y. He, "Bault diagnosis method based on self-adaptive stochastic resonance of genetic algorithm and VMD," *Journal of Mechanical Transmission*, vol. 162, Article ID 108018, 2018.
[32] J. M. Keller, M. R. Gray, and J. A. Givens, "A fuzzy K-nearest neighbor algorithm," *IEEE Transactions on Systems Man & Cybernetics*, vol. 15, no. 4, pp. 580–585, 2012.
[33] W. A. Smith and R. B. Randall, "Rolling element bearing diagnostics using the case Western reserve University data: a benchmark study," *Mechanical Systems and Signal Processing*, vol. 64–65, pp. 100–131, 2015.